Supplementary information to Elsässer et al.

Simulating ice core ^{10}Be on the glacial-interglacial timescale, *Clim. Past Discuss.*

S.1 The atmospheric transport model setup

S.1.1 Basics and model setup

The Global RAdioCarbon Exploration model (GRACE) is a two-dimensional box model of the global atmosphere airmass transport developed by Hesshaimer [1997] and substantially revised by Naegler [2005] and Levin *et al.* [2010]. Previous to its application for aerosol-bound radionuclides the model setup consisted of 28 boxes: 30° resolution boundary layer, free troposphere, lower, mid and high stratosphere. Within the work of Elsässer [2013], boundary layer latitudinal resolution was increased to 10° per box (see Fig. S.1) to simulate aerosol-bound radionuclides. All parameters of airmass transport have been calibrated using global observations of SF_6 and bomb ^{14}C. In addition, seasonal variations of airmass fluxes in the southern extra-tropics were calibrated by the ^{10}Be/^{7}Be ratio observed at Antarctic Neumayer Station. Details of the model setup such as the airmass transport calibration strategy are described in the supplementary information of Levin *et al.* [2010].

S.1.2 Atmospheric transport

The transport of different atmospheric constituents is based on tracer-calibrated airmass transport. Hence, the net transport of tracers follows

$$F_{ij}^{tracer}(t) = c_i^{tracer}(t) \cdot F_{ij}^{airmass}(t) - c_j^{tracer}(t) \cdot F_{ji}^{airmass}(t) \tag{S.1}$$

F_{ij} : Flux between box i and j
c_i: Tracer concentration in box i

Airmass transport comprises three different processes: Diffusive transport, Brewer-Dobson circulation and seasonal varying tropopause height. This setup results in a complex system of ordinary differential equations with time-dependent parameters, which is solved numerically using a Runge-Kutta method within the MATLAB/Simulink software package.

S.1.3 Radionuclide sources

Cosmogenic radionuclides

Production rate calculations of Usoskin & Kovaltsov [2008] (and Kovaltsov & Usoskin [2010]) as well as Masarik & Beer [2009] are implemented into the model. To this end production rate distributions in the atmosphere are calculated quantitatively as a function of solar activity and the geomagnetic field. In case of the Usoskin & Kovaltsov [2008] data, the dependency of the production distribution on the geomagnetic dipole field had to be inferred from cutoff rigidities (Pcutoff). In doing so we used the cutoff rigidity - latitude conversion given in Masarik & Beer [2009]

$$P_{cutoff} = 14.9 \cdot \frac{M(t)}{M_0} \cdot cos^4(\lambda) \tag{S.2}$$

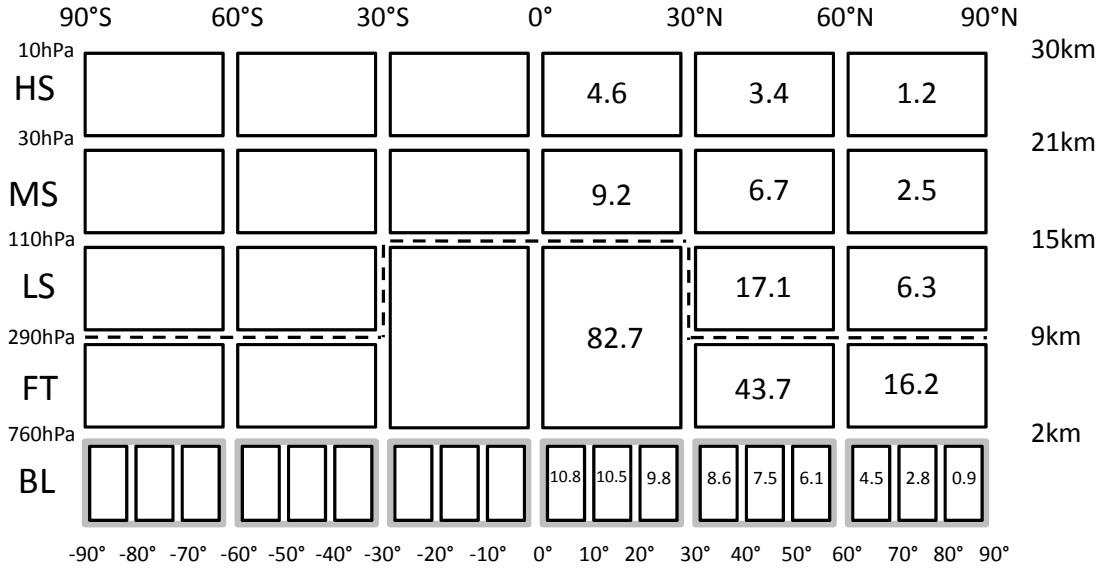

Figure S.1 The atmospheric transport model setup. Numbers in the different boxes denote the respective box airmass in 10^{16}kg. The airmass of the total atmosphere is 510 x 10^{16} kg. Note that the airmasses are symmetrical in both hemispheres. Grey boundary layer (BL) boxes display the model setup previous to this work. The additional Greenland Ice Sheet box is incorporated in the 70°N - 80°N box (see S.1.6 for details) and not shown. The Tropopause is depicted as dashed line.

Since our atmospheric model is two-dimensional, usage of more realistic cutoff rigidity - latitude conversion (e.g. Smart & Shea [2008]) would not significantly improve the model results. Production rates are given as a function of atmospheric depth. The here deployed atmospheric model setup actually covers atmospheric depths from 10 g cm^{-2} to 1023 g cm^{-2}. However, the full range of atmospheric depths (0-1030 g cm^{-2}) is used for production rate calculations in the model to capture the full atmospheric inventory of ^{7}Be and ^{10}Be with the model. In case of the polar boundary layer boxes (i.e. the Antarctic and Greenland ice sheets), the production is adapted to the overall shifted altitudes. To this end, mean altitudes of 3km (Antarctic plateau), 2km (Greenland Ice Sheet) and 1km (coastal Antarctica) as well as an overall polar boundary layer height of 1km is assumed. This correction results in a factor of three higher local production rate on the Antarctic plateau, a factor two in case of the Greenland Ice Sheet and 10% higher local production rate at coastal Antarctica. However, the effect on the local air concentration is much lower (final model calibration applied): 9% (17%) enhancement on the Antarctic plateau in case of ^{10}Be (^{7}Be) and 7% (16%) for the Greenland Ice Sheet, respectively. See also Elsässer [2013] for further details.

Anthropogenic bomb fission radionuclides

Anthropogenic bomb fission radionuclides entered the global atmosphere within extensive atmospheric nuclear bomb tests in the 20th century (see e.g. Junge [1963] for details). While more than 200 different radionuclides are produced within a nuclear test [Masarik, 2010], only a few of these are spread globally due to short radioactive and/or atmospheric lifetimes. The bomb fission radionuclides ^{137}Cs and ^{90}Sr (radioactive lifetimes 43.5 years and 41.5 years) have been extensively measured on the global scale and thus offer a valuable tool for calibration of the model radionuclide sink. Implementing ^{137}Cs and ^{90}Sr in the model, we follow results of the UNSCEAR [2000] report. The time-dependent global production distribution is based on the composite time-series of single atmospheric nuclear bomb tests and their respective characteristics. The amount of nuclides produced within a single test is scaled linearly from its respective total explosive force using the fission yields from UNSCEAR [2000]. The amount of fission nuclides spread globally, regionally and locally as well as their vertical atmospheric distribution is based on the assumptions given in UNSCEAR [2000]. Local and regional production rates are not taken into account since these fission yields are not assumed to spread over the whole latitudinal band (and thus cannot be simulated with a 2-dimensional model approach). Eventually, this assumption is reasonable if the sampling sites (for model calibration and validation) are not positioned in the regional vicinity of the test sites.

Terrigenic radionuclides

The natural, terrigenic radionuclide ^{210}Pb (radioactive livetime: 32 years) emerges from ^{222}Rn decay in the atmosphere. Its atmospheric source distribution thus contrasts those from cosmogenic and anthropogenic radionuclides. For this reason, atmospheric sink processes (like wash-out by precipitation) of ^{210}Pb generally differ from those of cosmogenic radionuclides. However, since polar areas lack local ^{222}Rn sources, polar ^{210}Pb underlies atmospheric transport processes similar to cosmogenic or bomb fission radionuclides (i.e. higher atmosphere is the main source region). Greenland and Antarctic ^{210}Pb measurements may therefore support the model calibration of ^{10}Be transport and deposition processes in polar areas. For simulating the global ^{210}Pb source we implemented global ^{222}Rn sources into the model setup and calculated ^{210}Pb online from ^{222}Rn decay. Since ^{222}Rn sources show a strong land-ocean

contrast, it is not intended to correctly reproduce boundary layer measurements of ^{222}Rn activity concentration with this low-resolution, two-dimensional model. This is even more true, since activity concentrations of short-lived ^{222}Rn (radioactive lifetime 5.5 days) in the atmospheric boundary layer are driven by small-scale atmospheric transport processes. However, the model setup should be capable to realistically simulate the global atmospheric ^{222}Rn inventory and thus the global ^{210}Pb source. A constant ^{222}Rn flux of 1 atom cm^{-2} s^{-1} is implemented into the tropical boundary layer boxes and the flux is linearly reduced from 30°N to 70°N according to Conen & Robertson [2002].

S.1.4 Aerosol gravitational settling

(Sub-micron) Aerosols are subject to gravitational settling. While this effect is of minor importance in the troposphere, it may have a significant influence on the aerosol transport in less turbulent stratospheric layers of the atmosphere. The model setup was upgraded with an aerosol gravitational settling module by estimating the (constant) terminal gravitational settling velocity v_t using the Stokes-Cunningham-friction force and the gravitational force (e.g. Schery [2001]; Lazarev [2003]).

$$v_t = \frac{2r_{aerosol}^2 \cdot C \cdot g \cdot \rho_{aerosol}}{9\nu} \tag{S.3}$$

with
v_t= terminal gravitational settling velocity
$r_{aerosol}$ = mean aerosol radius
$\rho_{aerosol}$= mean aerosol density
C = Cunningham slip correction factor
ν =viscosity of air
g = gravitational acceleration

The Cunningham slip correction factor is taken from Allen & Raabe [1985]. Equation S.3 shows, that a critical parameter in the estimation of aerosol gravitational settling is the aerosol diameter. Based on measurements of ^{7}Be Air Activity Median Aerodynamic Diameters (AMAD) in the boundary layer (e.g. Papastefanou [2008]) we found that aerosol gravitational settling does not significantly alter the tropospheric residence time of ^{10}Be (see details in Elsässer [2013]). In the stratosphere we estimate radionuclide gravitational settling fluxes based on a roughly estimated radionulide radius of 0.1 μm [Junge, 1963; Martell, 1966].

S.1.5 Global radionuclide sinks

Radionuclide (and related sub-micron aerosol) deposition is implemented into the boundary layer boxes which serve as the only radionuclide sink besides radioactive decay. In every box i, the deposition is separated into a wet and a dry deposition fraction and depends on (i) the radionuclide air activity concentration c^i, (ii) the monthly mean precipitation rate P^i, (iii) the scavenging ratio (ratio between radionuclide rain and air concentration) ϵ^i as well as (iv) the dry deposition velocity (v_{dry}):

$$J^i(t) = J^i_{dry}(t) + J^i_{wet}(t) = (v_{dry} + \epsilon^i \cdot P^i(t)) \cdot c^i_{air}(t) \tag{S.4}$$

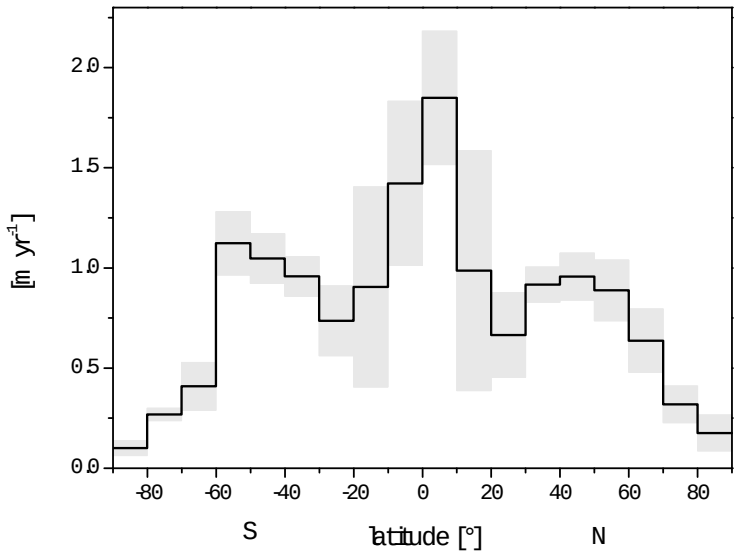

Figure S.2 Precipitation in the GRACE model based on Adler *et al.* [2003]. Grey bands denote standard deviation of seasonal variability. In polar areas precipitation rates have been revised using data from Arthern *et al.* [2006], Bales *et al.* [2001] and EML-Fallout [2010].

While c_{air} is calculated online during each model run, the parameters $P^i(t)$, $v_{dry}(t)$ and $\epsilon^i(t)$ are defined within model initialization. All parameters can be varied on the seasonal and multiannual timescale. However, v_{dry} and ϵ are kept constant except some exceptions (see fine tuning, below).

Precipitation and dry deposition

Precipitation rates are compiled from the Global Precipitation Climatology Project (GPCP) [Adler *et al.*, 2003] which is based on satellite data and surface rain gauge observations over the time period 1979-2001 (see Fig. S.2). Precipitation varies on a seasonal scale. For observational period model runs, inter-annual changes are neglected but precipitation is modulated in case of the multi-millennial simulations (see Sect. 2.3.2). In case of the 80°-90°S Antarctic ice sheet box we reduce the mean precipitation rate from Adler *et al.* [2003] by 25% which results in a mean precipitation rate of 10 cm year^{-1}. This is in line with data from Arthern *et al.* [2006] who report on 9 cm year^{-1} for the 80°-90°S region. In case of coastal Antarctica (i.e. 70°-80°S), Adler *et al.* [2003] give a mean precipitation rate of 27cm year^{-1} which is broadly in line with observations at the German Neumayer station. For the Antarctic Peninsula box we used observed monthly precipitation rates from the Chilean station (Deception Island, 62°56'S, 60°36'W) within the EML fallout program (median: 40 cm year^{-1}). Finally, the mean precipitation rate in the Greenland ice sheet box is taken from Bales *et al.* [2001] (30cm year^{-1}, no seasonal modulation). The dry deposition velocity is assumed to be globally constant at 0.1 cm s^{-1}. This value results from our polar ^{10}Be air firn transfer model but lies in the range of suggested (global-scale) dry deposition velocities for aerosol-bound radionuclides [Sportisse, 2007].

Scavenging ratios and boundary layer - free troposphere diffusive air mass transport

The scavenging ratios (related to the scavenging efficiency) and the diffusive airmass exchange of every single boundary layer box with the related free troposphere is calibrated using respective radionuclide measurements. To this end we used global-scale observations of ^{90}Sr deposition as well as ^{137}Cs and ^{90}Sr air concentration within the following calibration strategy:

1. Initial values: Initial values of the scavenging ratio are obtained from contemporaneous measurements (long-term time series) of ^{90}Sr boundary layer air activity concentration and the ^{90}Sr deposition flux at several monitoring stations on the global scale [EML-SASP, 2010; EML-Fallout, 2010]. Scavenging ratios show lower values around 2-3 $\cdot$ 10^5 [atoms SCM^{-1} / atoms SCM^{-1}] at low latitudes sites and higher values up to 8 $\cdot$ 10^5 [atoms SCM^{-1} / atoms SCM^{-1}] at higher latitudes. The initial value for the BL-FT diffusive airmass transport is provided by the GRACE model calibration [Levin *et al.*, 2010].

2. Boundary layer - free troposphere coupling: Model results of time-integrated ^{90}Sr deposition (inventory) in the 18 boundary layer boxes are adapted to observational data given in UNSCEAR [2000] (see Fig. S.3a) by varying the diffusive boundary layer - free troposphere air mass exchange. In case of the Antarctic Peninsula box, we use mean measured ^{137}Cs and ^{90}Sr inventories from Roos *et al.* [1994] since UNSCEAR [2000] data is extrapolated. Ice sheet boxes have a different calibration strategy (see S.1.6).

3. Scavenging ratio: Model results of the ^{90}Sr activity concentration in the 18 boundary layer boxes are adapted to observed time series (compilation from 71 globally distributed sampling sites; [Kolb, 1992; EML-SASP, 2010]) by varying the specific scavenging ratio for every box (see Fig. S.3b and S.3c for exemplary data). For the most northern polar box (80°-90°N), data from 70°-80°N (Thule and Kap Tobin Station, Greenland; Barrow, Alaska) is used. Since phase differences in seasonal cycles may distort the comparison of monthly data, a Gaussian smooth of model and measurements data is used to compare both time series. In doing so, we use a filter which dampens the seasonal cycle amplitude to 0.1% and air concentration measurements in the 1960-1980 period.

4. Iteration of 2. and 3.

5. Fine tuning (see below)

6. Iteration of 2. and 3.

While this first-order calibration explains much of the radionuclides' variability, several effects have to be accounted for within a fine tuning of the model aerosol sinks:

- Arctic haze phenomenon: Comparison of ^{90}Sr atmospheric activity concentration and deposition flux measurements at Thule (Greenland coast, Arctic basin) reveals, that the respective ^{90}Sr deposition velocity is up to an order of magnitude higher during July and August compared to the rest of the year. This effect contributes to the 'Arctic haze phenomenon' (e.g. Stohl [2006]) and cannot be accounted for by solely using accumulation rate variations. Hence, we modulate the scavenging ratio of the northern polar boxes (except of the Greenland ice sheet) with a seasonal variation based on

the (^{90}Sr-derived) deposition velocities from Thule station (77°N, 69°W) time series. Resulting scavenging ratios in July and August are up to a factor of 37 higher than during the rest of the year.

- Diffusive airmass exchange between polar ice sheets and coastal areas: We inhibit the diffusive air mass exchange between the ice sheet boxes with the surrounding polar boxes (Arctic basin, Antarctic Peninsula and surrounding ocean). Indeed this is a rough oversimplification. However, the major differences in measured radionuclide seasonality and mean air concentrations (e.g. Dibb & Jaffrezo [1993]; Elsässer *et al.* [2011]) indicate that these air masses substantially differ. Moreover, the dryness of the polar ice sheets point to minor exchange with the surrounding maritime air masses. Unidirectional fluxes from the ice sheets to the ocean according to katabatic drainage is accounted for by the Brewer-Dobson fluxes in the model setup.

- Tropical seasonality: In case of tropical boundary layer boxes, the seasonal cycle of ^{90}Sr air concentration model results are quite different from measurements. Indeed, heavy meteorological events like monsoon rain may significantly influence the aerosol sink. Certainly, precipitation regimes of the tropics (e.g. regional shift of the Inter-Tropical Convergence Zone) are not captured by the model's 10° resolution. To account for this effect, scavenging ratios of the tropical boxes are modulated with a seasonal cycle to fit the ^{90}Sr seasonality. However, this may be an unrealistic extrapolation of local conditions at single measurement sites to the total boundary layer box.

- Ice sheet boxes: The calibration strategy of the polar ice sheet boxes differs since observations of bomb fission nuclides are sparse. Details are given in S.1.6.

The fitted model results together with reference data is shown exemplary in figure S.3 (further figures are given in Elsässer [2013]). Figures S.4 shows details of the resulting model radionuclide sink parameterization. We find higher radionuclide boundary layer residence times in the subtropics and polar areas which is in line with expectation. The efficiency of precipitation to remove aerosol-bound radionuclides (related to the scavenging ratio) is highest in mid latitudes and significantly lower in polar latitudes. In combination with lowest vertical mixing and low precipitation rates, the polar areas thus constitute the lowest sink region of aerosol-bound radionuclides in the global atmosphere.

Estimation of uncertainty

The calibration of the radionuclide sink is backed-up with an estimation of uncertainty. Aerosol-bound radionuclides are subject to significant meteorological noise. In case of natural radionuclides, long time series provide significant results of the radionuclide climatology. In case of anthropogenic bomb fission nuclides, major temporal variability of the atmospheric sources hamper the observation of climatological averaged results. We therefore apply different scenarios on data handling of the atmospheric ^{90}Sr and ^{137}Cs measurements to account for meteorological noise. In detail we vary the timeframe under investigation together with the smoothing strategy. Resulting error ranges are given in Fig. 1 and S.4.

S.1.6 The ice sheet boxes

With respect to both, the focus of the study being on ice-core ^{10}Be, but also the comparatively low observational data basis, polar areas require special consideration. In case of Antarctica,

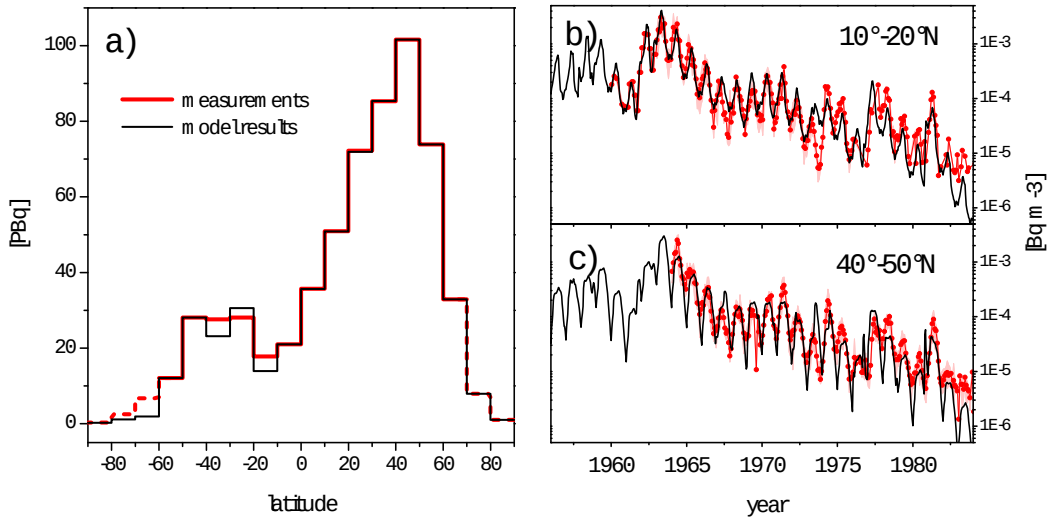

Figure S.3 ^{90}Sr measurements (red) used for model calibration together with the fitted model results (black). a) ^{90}Sr soil inventory (time integrated deposition flux) based on UNSCEAR [2000]. Note that polar observations (dashed red) are extrapolated values. b) and c) Exemplary ^{90}Sr air concentration time series for two boxes [EML-SASP, 2010]. Red shaded areas show maximum and minimum values in case of several data sets combined. ^{90}Sr data is augmented by ^{137}Cs measurements using a fixed ratio of 1.524 [UNSCEAR, 2000].

Elsässer *et al.* [2011] find comparable mean air activity concentrations of ^{7}Be and ^{210}Pb at coastal Antarctica and the high Antarctic plateau, but considerably lower concentrations at Antarctic Peninsula sampling sites. The 10° model resolution is thus applicable to simulate aerosol-bound radionuclides in the southern polar boundary layer since the three boundary layer boxes broadly represent the three different Antarctic climate realms:

- The high Antarctic plateau: 90°S - 80°S
- Coastal Antarctica: 80°S - 70°S
- Antarctica Peninsula: 70°S - 60°S

On the contrary, the Greenland ice sheet atmospheric boundary layer represents a small part of the Arctic boundary layer, only. However, similar to Antarctica, measurements of atmospheric radionuclides indicate that the Greenland ice sheet air mass differs from the Arctic basin [Dibb & Jaffrezo, 1993; Dibb, 2007]. Therefore an additional Greenland ice sheet box was incorporated into the northern mid polar box (70°N-80°N), reducing its airmass by 15%. The airmass of the Greenland ice sheet boundary layer box (4.1×10^{15} kg) represents 5% of the polar boxes and 0.08% of the global airmass, only, allowing for a virtually independent calibration of its transport and deposition parameters.
In both cases, Greenland and Antarctica, it is not feasible to use bomb-fission radionuclides for the calibration of the polar radionuclide sinks since their observational data basis is low. We therefore use the results of the ^{10}Be air-firn transfer model (see Sect. 2.2) for an estimation of dry deposition velocities and scavenging ratios. In doing so, the remaining parameter for every boundary layer box is the diffusive airmass transport with the respective free polar

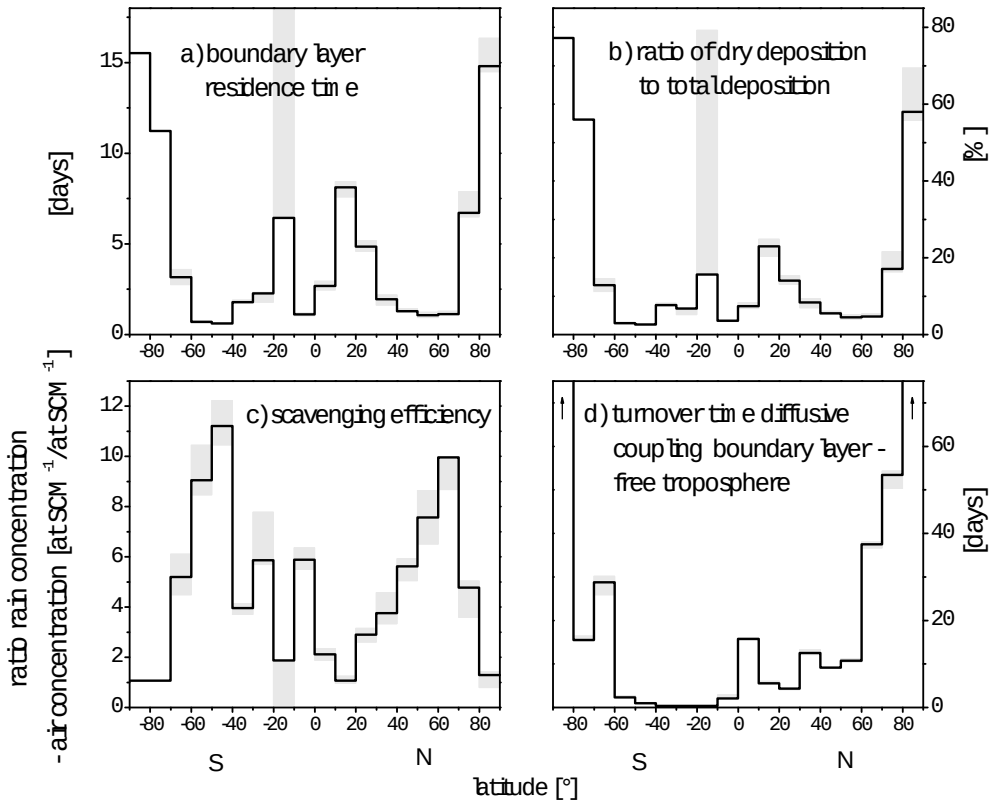

Figure S.4 Parameterization of the model's radionuclide sink resulting from calibration with observational bomb fission radionuclide data. Grey-shaded areas depict estimation of uncertainty from bomb-fission nuclides based model calibration. Uncertainty of dry deposition is not taken into account. Note that the parameters of the Greenland ice sheet box are not shown but given in Table S.1.

troposphere. So far we apply measured overall mean ^{7}Be activity air concentrations for the calibration of this diffusive BL-FT coupling. This strategy precludes model validation with ^{7}Be in polar areas but ensures high-grade model calibration. Finally we implement and calibrate the seasonality of the polar boundary layer inversion strength. Elsässer *et al.* [2011] showed that seasonal variations of the boundary layer inversion strength are a prominent feature of the vertical transport of radionuclides in the polar atmosphere. Hence, the diffusive boundary layer - free troposphere air-mass transport (of the Antarctic (70°S - 90°S) and Greenland ice sheet boxes) is modulated with a seasonal cycle. For this purpose model results of the relative ^{210}Pb seasonal cycle in boundary layer air were adapted to ^{210}Pb air concentration measurements. In case of the Antarctic Ice Sheet box (80°-90°S) the diffusive air mass exchange is largest during January and December (220% and 420% of the overall mean) and diminished in May. For coastal Antarctica (70°-80°S) the seasonal cycle amplitude is smaller (up to 30%). In case of the Greenland ice sheet box, diffusive air mass exchange with the free polar troposphere shows a bimodal maximum in April (40% of the overall mean) and October (25% of the overall mean) following ^{210}Pb observations at Greenland Summit from Dibb [2007]. Decisive model parameters of the ice sheet boxes are given in Table S.1.

S.1.7 Additional model validation

Figure S.5 shows the model results of the normalized ^{7}Be seasonal cycles in the boundary layer boxes compared to respective measurements. Each data set is normalized to the respective overall mean ^{7}Be air activity concentration. The model-measurement comparison reveals that the model captures the ^{7}Be seasonal cycle in the atmospheric boundary layer regarding phase and amplitude. The agreement is remarkable in case of mid- and polar latitudes but less in case of lower latitudes.

S.2 ^{10}Be air-firn-transfer model

S.2.1 ^{10}Be measurements

^{10}Be is measured using Accelerator Mass Spectrometry (AMS). The processing of ice samples and ^{10}Be extraction chemistry was performed at Heidelberg laboratory. The extraction procedures and AMS target preparation followed standard practice [Wagner, 1998; Stone *et al.*, 2004]. Measurements of ^{10}Be have been performed at the ETH Zurich (Greenland samples) as well as in the VERA laboratory in Vienna (Antarctic samples). All measurements refer to the ETH S555 standard material but are recalibrated to Nishiizumi *et al.* [2007].

S.2.2 Recalibration and correction of published ^{10}Be measurements

Quantitatively comparing mean ^{10}Be ice concentrations from different surveys, two issues require recalibration: (i) Different AMS laboratories use different measurement calibration standards and (ii) observed ^{10}Be ice concentrations cover different periods of time and are thus modulated by different conditions of cosmogenic production variability. With respect to (i), we use results from Nishiizumi *et al.* [2007] and Kubik & Christl [2010] to revise published measurements. This recalibration involves correction of different measurements ranging from -9.6% to +4.1%. Regarding (ii) we apply our atmospheric ^{10}Be model together with records of the cosmogenic production variability. To do so, we calculated the solar activity parameter

Table S.1. Details of the ice sheet parameterization in the atmospheric box model setup.

Parameter	Greenland	Antarctic coast (70°S-80°S)	Antarctic high plateau (80°S-90°S)
Airmass [kg]	4.1×10^{15}	2.8×10^{16}	9.3×10^{15}
Area [km^2]	1.71×10^6	11.5×10^6	3.86×10^6
Boundary layer height [km]	2	2	2
Turnover time diffusive BL-FT air mass transport [years]	0.27	0.042	0.36
Scavenging ratio (volume-based) [atoms m_{air}^{-3} / atoms m_{snow}^{-3}]	3.1×10^5	1.1×10^5	1.1×10^5
Dry deposition velocity [cm s^{-1}]	0.10	0.12	012
Snow accumulation rate [m yr^{-1}]	0.30	0.27	0.10
Ratio dry to total deposition (observational period)	31%	56%	77%
^{10}Be residence time [days]	6	11	16

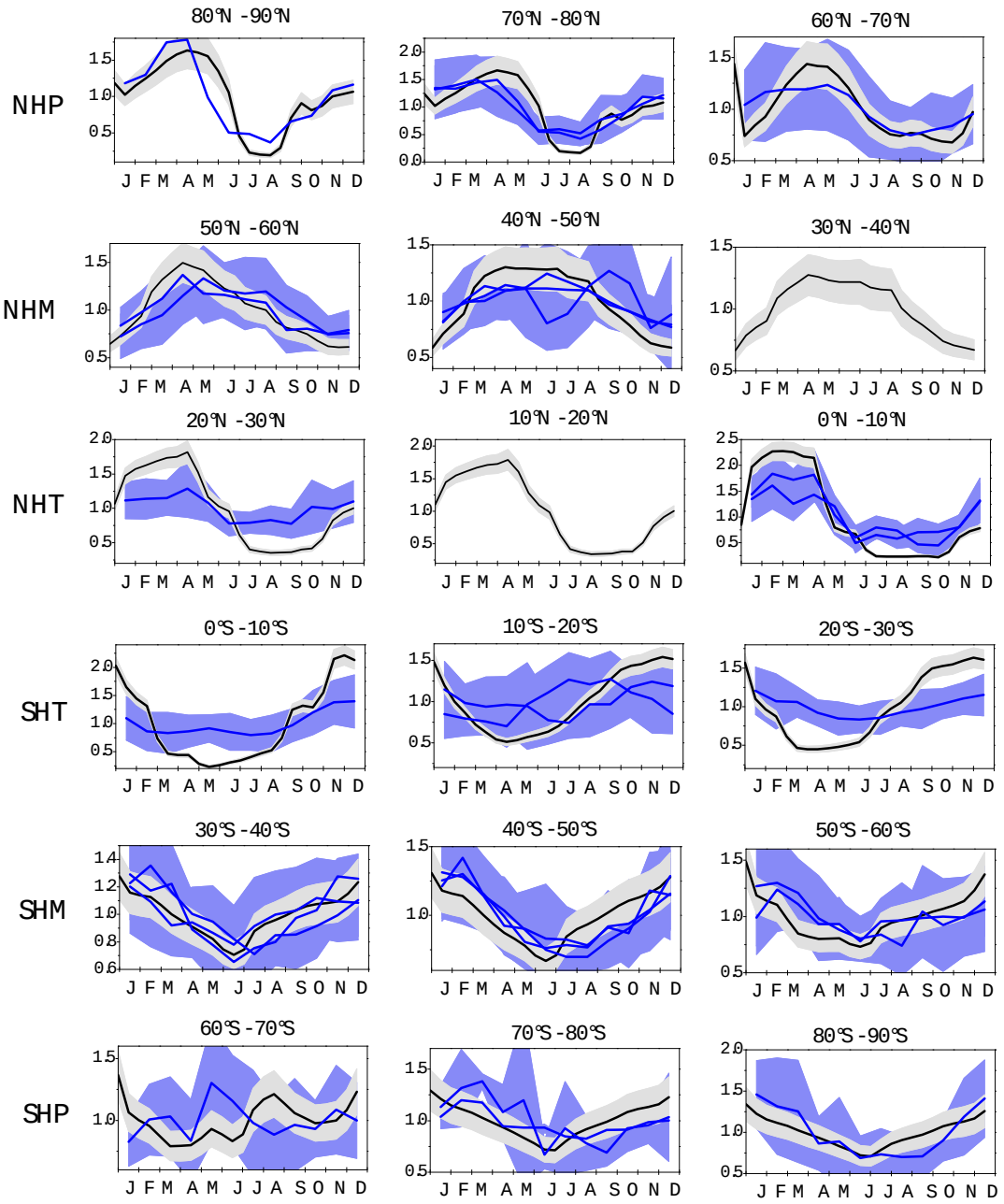

Figure S.5 Model-measurements comparison of the ^{7}Be seasonal cycle in boundary layer air. Black lines show stacked model results for the 1950-2000 period and grey bands respective standard deviation from multi-annual variability (due to production changes). Model results and measurements are normalized to the respective overall mean. Measurements [EML-SASP, 2010; Kolb, 1992; Dibb *et al.*, 1994; Wershofen & Arnold, 2005; Elsässer *et al.*, 2011] are shown as blue lines (stacked monthly mean values) and blue shaded areas (standard deviation). Measurements from multiple sampling sites representative for a 10° box are shown separately (multiple blue lines).

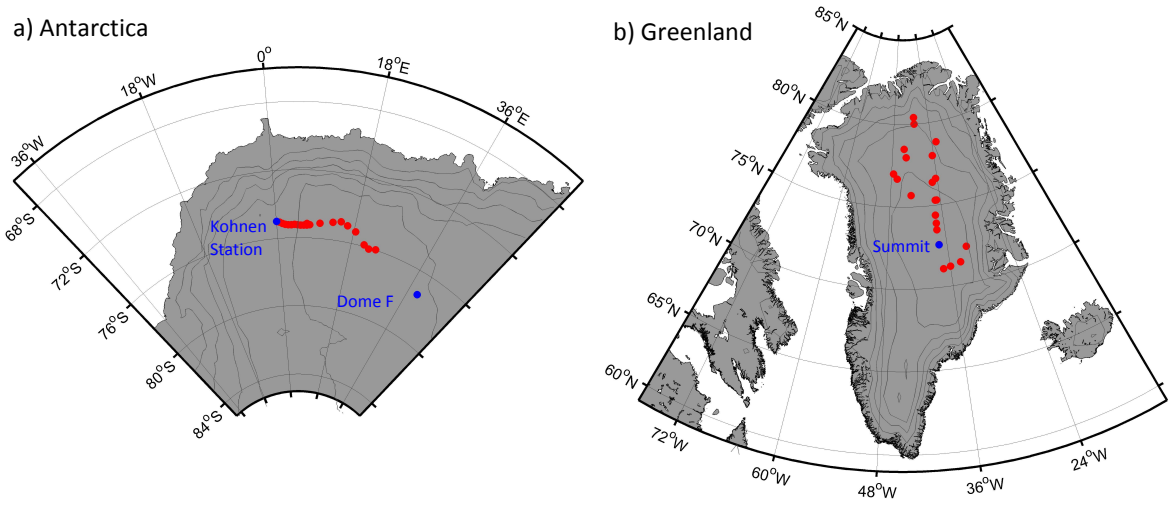

Figure S.6 Maps of the Greenland and Antarctic sampling sites for the ^{10}Be measurements shown in Fig. 5. Details are given in S.2.3 and S.2.4 as well as Stanzick [2001] and Elsässer [2013].

from the ^{14}C INTCAL09 record [Reimer *et al.*, 2009] using a basic Siegenthaler-Oeschger carbon cycle model [Oeschger *et al.*, 1975; Siegenthaler, 1983] and a record of geomagnetic dipole changes [Laj *et al.*, 2004] (^{14}C production rate calculations from Masarik & Beer [1999] - see Elsässer [2013] for details). For the most recent period, solar activity is augmented by recent neutron monitor-based reconstruction from Usoskin *et al.* [2011]. Eventually, we use this solar activity record together with reconstructed geomagnetic variability [Laj *et al.*, 2004] to drive the atmospheric ^{10}Be model. The model results for the ^{10}Be air concentration in the boundary layer above the ice sheets are used to correct for different states of atmospheric production recorded in the different ^{10}Be ice core data.

S.2.3 The Greenland EGIG and NGT traverses

The Greenland ^{10}Be traverse measurements comprise samples from the EGIG ("Expedition Glaciologique Internationale au Groenland") and NGT ("North Greenland Traverse") surveys in 1990-1992 and 1993-1995, respectively (Stanzick [2001] - see Fig. S.6). The EGIG traverse transect samples the Greenland ice sheet in east-west direction around 69°-73°N (e.g. Fischer & Wagenbach [1996]). The NGT traverse spans 2000km starting from Greenland Summit alongside of the northern ice divide up to 80.4°N and returns to 75°N in western direction (see details in Fischer [1997] and Stanzick [2001]). In summary, ^{10}Be measurements within both traverses sample altitudes ranging from 2010m up to 3137m. ^{10}Be measurements were accomplished at the ETH Zurich AMS laboratory. For the present study we re-calibrated the measurements for a new AMS calibration standard (see S.2.2). Determination of accumulation rates is based on different methods of dating and layer counting [Fischer, 1993; Stanzick, 2001]). For ten measurements individual information on the uncertainty of the determined accumulation rate was missing and an overall mean accumulation rate uncertainty of 10% was deployed.

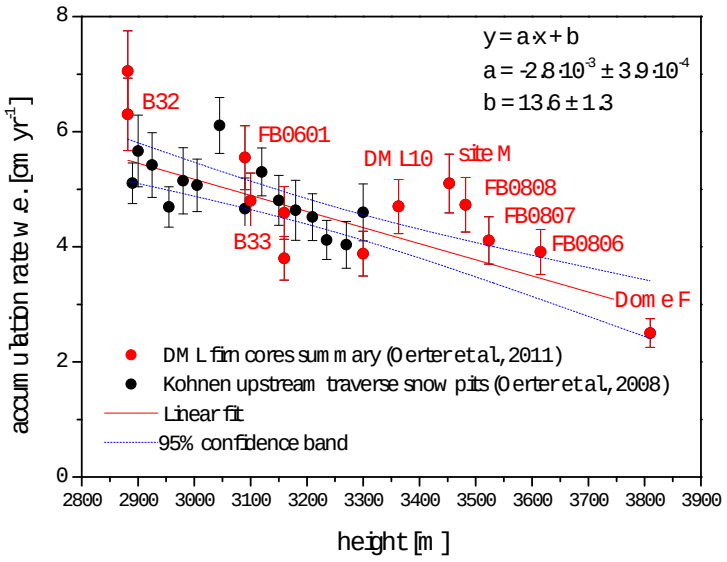

Figure S.7 Compilation of different snow accumulation rate measurements in the realm of the Kohnen upstream and JASE traverses [Oerter *et al.*, 2008, 2011]. The mean accumulation rates show a significant relation to the altitudes at the respective sampling sites. Kohnen upstream traverse snow pits cover 9-13 years around the year 2000. Firn cores cover at least 90 years.

S.2.4 The Antarctic Kohnen upstream and JASE traverses

The Antarctic Kohnen upstream traverse was performed by the Alfred-Wegener-Institute for Polar and Marine Research in 2006. Within this survey, snow pit samples along a 280km traverse upstream from Kohnen Station (EDML drilling site) were collected (see Fig. S.6). Sampling sites comprise altitudes from 2890m to 3300m a.s.l.. 15 snow pits were measured for mean ^{10}Be concentration. In 2007/2008 a Japanese-Swedish expedition (JASE) allowed for augmenting the ^{10}Be measurements for another 9 samples ranging from the end of the Kohnen upstream traverse roughly 400km towards Dome F station (highest sampling site: 3615m - see Fig. S.6). In comparison to the Greenland traverses, the accumulation rates at the Antarctic sampling sites are a factor of 2.5 - 3.8 lower. Due to the drier conditions, direct measurement of annual layer thickness in snow pits (e.g. based on counting of δ^{18}O seasonal cycles [Oerter *et al.*, 2008]) is challenging. To reduce uncertainty, we therefore infer accumulation rates for single sampling sites from an overall relation between elevation and snow accumulation. To do so, we compile snow pit and firn core accumulation rate measurements in the realm of the Kohnen upstream and JASE traverses [Oerter *et al.*, 2008, 2011]. Figure S.7 shows the measured accumulation rates plotted against the altitude of the respective sampling sites. For the determination of long-term accumulation rates based on firn cores, a mean uncertainty of 10% is assumed. We use the linear fit to this altitude-accumulation relation to infer overall mean accumulation rates at our ^{10}Be sampling sites. The uncertainty of these accumulation rate estimations are based on the 95% confidence band of the linear fit (see Fig. S.7).

S.3 Greenland Summit ^{10}Be measurements and model results

S.3.1 GRIP accumulation rate profile and the GICC05modelext timescale

For the long-term model attempt we applied new calculations of the GRIP snow accumulation rate changes. To this end we used the NGRIP GICC05modelext timescale [Vinther *et al.*, 2006; Rasmussen *et al.*, 2006; Andersen *et al.*, 2006; Svensson *et al.*, 2008; Wolff *et al.*, 2010] which is transferred to GRIP using partly unpublished match points of mainly volcanic origin between the NGRIP and GRIP ice cores [Rasmussen *et al.*, 2008; Blockley *et al.*, 2012; Svensson *et al.*, 2013; Seierstad *et al.*, 2014]. From the resulting GRIP annual layer thickness profile we calculated snow accumulation rates by correcting for ice-flow induced layer thinning. Here, we used an accumulated vertical strain profile from the so-called ss09sea Dansgaard-Johnsen ice flow model (Johnsen *et al.* [2001], A. Svensson, pers. communication). Reconstructed GRIP accumulation rates from Andersen *et al.* [2006] have been used for the most recent time period. The resulting record of reconstructed snow accumulation rate at the GRIP site is shown in Fig. 7a. Most significant differences between the revised GRIP accumulation rate records and earlier calculations [Johnsen *et al.*, 1995] occur in the (15-20)kyr b2k period.

S.3.2 GRIP and GISP2 measurements

Measurements for Greenland Summit measurements-model comparison comprise published data from the GISP2 [Finkel & Nishiizumi, 1997] and GRIP [Yiou *et al.*, 1997; Wagner *et al.*, 2001; Muscheler *et al.*, 2004] ice cores. Both ice core records have been transferred to the GICC05modelext timescale using the partöy unpublished match points between NGRIP, GRIP and GISP2 ice cores (see S.3.1). The measurements have been corrected for ^{10}Be decay and different AMS calibration standards using results from Nishiizumi *et al.* [2007] and Kubik & Christl [2010]. Moreover, different sample processing strategies of different laboratories required further correction of the data: Processing of melted ice samples comprised filtering to account for ^{10}Be related to micrometeorites [Yiou *et al.*, 1997]. However, the application of different filter pore sizes in different laboratories requires alignment of the different data sets. Investigating the filter residue of small pore size filters, Baumgartner *et al.* [1997] report on a ^{10}Be fraction of 20% reserved in the filters of samples from the glacial period. The authors argue that this portion of ^{10}Be could be related to aeolian dust. However, the effect of recycled ^{10}Be is not resolved definitely (see Baumgartner *et al.* [1997] for details). Different studies thus reported either (i) on the total ^{10}Be content of the (large pore size) filter plus filtrate (GISP - Finkel & Nishiizumi [1997]), (ii) on the ^{10}Be filtrate concentration only using large pore size filters (GRIP - Yiou *et al.* [1997]), or (iii) on the ^{10}Be filtrate concentration only using small pore size filters (GRIP - Yiou *et al.* [1997]). For the model comparison (shown in Fig. 7) we follow Muscheler *et al.* [2004] and scale glacial period measurements based on small pore size filtration by 25%. Unfortunately, the application of small pore size filters and thus correction of the measurements is not randomly distributed over the time series. In detail, virtually all measurements in (37.8 - 49.4)kyr b2k and (67.5-75)kyr b2k but no measurements in (0-27.5)kyr b2k are corrected for the filtration effect. In the (27.5-37.8)kyr b2k period most measurements (except during a 1000years interval around 34.3kyr b2k) are corrected. During (49.4-67.5)kyr b2k multi-centennial periods with corrected and uncorrected measurements alternate. It is important to highlight that these periods do not coincide with periods of major model-measurements differences (see Sect. 3.1). Indeed, the

correction of the GRIP records further reduces the difference to the GISP2 record which refers to both, ^{10}Be from filtration residue and filtrate (see Muscheler *et al.* [2004]). However, the somewhat empirical (and time-dependent) correction introduces some additional uncertainty to the measured ^{10}Be.

References

Adler, R.F., G.J., Huffman, Chang, A., Ferraro, R., Xie, P.P., Janowiak, J., Rudolf, B., Schneider, U., Curtis, S., Bolvin, D., Gruber, A., Susskind, J., Arkin, P., & Nelkin, E. 2003. The version-2 global precipitation climatology project (GPCP) monthly precipitation analysis (1979-present). *Journal of Hydrometeorology*, **4**, 1147–1167.

Allen, M.D., & Raabe, O.G. 1985. Slip correction measurements of spherical solid aerosol particles in an improved Millikan apparatus. *Aerosol Science and Technology*, **4**, 269–286.

Andersen, K.K., Svensson, A., Johnsen, S.J., Rasmussen, S.O., Bigler, M., Röthlisberger, R., Ruth, U., Siggaard-Andersen, M.-L., Steffensen, J.P., Dahl-Jensen, D., Vinther, B.M., & Clausen, H.B. 2006. The Greenland Ice Core Chronology 2005 15-42 ka. Part 1: Constructing the time scale. *Quaternary Science Reviews*, **25**, 3246–3257.

Arthern, R.J., Winebrenner, D. P., & Vaughan, D.G. 2006. Antarctic snow accumulation mapped using polarization of 4.3-cm wavelength microwave emission. *Journal of Geophysical Research*, **111**, D06107.

Bales, R.C., McConnell, J.R., Mosley-Thompson, E., & Csatho, B. 2001. Accumulation over the Greenland ice sheet from historical and recent records. *Journal of Geophysical Research*, **106(D4)**, 33,813–33,825.

Baumgartner, S., Beer, J., Wagner, G., Kubik, P., Suter, M., Raisbeck, G.M., & Yiou, F. 1997. ^{10}Be and dust. *Nuclear Instruments and Methods in Physics Research B*, **123**, 296–301.

Blockley, S.P.E., Lane, C.S., Hardiman, M., Rasmussen, S.O., Seierstad, I., Steffensen, J.P., Svensson, A., Lotter, A.F., Turney, C.S.M., & Ramsey, C. Bronk. 2012. Synchronisation of palaeoenvironmental records over the last 60,000 years, and an extended INTIMATE event stratigraphy to 48,000 b2k. *Quaternary Science Reviews*, **36**, 2–10.

Conen, F., & Robertson, L.B. 2002. Latitudinal distribution of radon-222 flux from continents. *Tellus*, **54B**, 127–133.

Dibb, J.D., Meeker, L. D., Finkel, R. C., Southon, J. R., Caffee, M. W., & Barrie, L. A. 1994. Estimation of stratospheric input to the Arctic troposphere: ^{7}Be and ^{10}Be in aerosols at Alert, Canada. *Journal of Geophysical Research*, **99**, 12,855–12,864.

Dibb, J.E. 2007. Vertical mixing above Summit, Greenland: Insights into seasonal and high frequency variability from the radionuclide tracers ^{7}Be and ^{210}Pb. *Atmospheric Environment*, **41(24)**, 5020–5030.

Dibb, J.E., & Jaffrezo, J.-L. 1993. Beryllium-7 and lead-210 in aerosol and snow in the Dye 3 Gas, Aerosol and Snow Sampling Program. *Atmospheric Environment*, **27A**, 2751–2760.

Elsässer, C. 2013. *Exporation of ^{10}Be ice core records using a climatological model approach: Cosmogenic production versus climate variability.* PhD thesis, University of Heidelberg, Heidelberg, Germany.

Elsässer, C., Wagenbach, D., Weller, R., Auer, M., Wallner, A., & Christl, M. 2011. Continuous 25-years aerosol records at coastal Antarctica: Part 2. Variability of the radionuclides ^{7}Be, ^{10}Be and ^{210}Pb. *Tellus*, **63B**.

EML-Fallout. 2010. *Fallout Programm.* Environmental Measurements Laboratory (EML): http://www.nbl.doe.gov/htm/EML_Legacy_Website/databases.htm. Access 2010.

EML-SASP. 2010. *Surface Air Sampling Programm.* Environmental Measurements Laboratory (EML): http://www.nbl.doe.gov/htm/EML_Legacy_Website/databases.htm. Access 2010.

Finkel, R.C., & Nishiizumi, K. 1997. Beryllium 10 concentrations in the Greenland Ice Sheet Project 2 ice core from 3-40 ka. *Journal of Geophysical Research*, **102(C12)**, 26,699–26,706.

Fischer, H. 1993. *Räumliche und zeitliche Verteilung glaziometeorologischer, isotopischer und chemischer Firnparameter im Ausflußgebiet Zentralgönland.* Diploma thesis, Institut für Umweltphysik, University of Heidelberg.

Fischer, H. 1997. *Räumliche Variabilität in Eiskernzeitreihen Nordostgrönlands.* PhD thesis, Institut für Umweltphysik, University of Heidelberg.

Fischer, H., & Wagenbach, D. 1996. Large-scale spatial trends in recent firn chemistry along an east-west transect through central Greenland. *Atmos. Environ.*, **30(19)**, 3227–3238.

Hesshaimer, V. 1997. *Tracing the global carbon cycle with bomb radiocarbon,.* PhD thesis, University of Heidelberg, Heidelberg, Germany.

Johnsen, S.J., Dahl-Jensen, D., Dansgaard, W., & Gundestrup, N. 1995. Greenland paleotemperatures derived from GRIP bore hole temperature and ice core isotope profiles. *Tellus*, **47B**, 624–629.

Johnsen, S.J., Dahl-Jensen, D., Gundestrup, N., Steffensen, J.P., Clausen, H.B., Miller, H., Masson-Delmotte, V., Sveinbjörnsdóttir, A.E., & White, J. 2001. Oxygen isotope and palaeotemperature records from six Greenland ice-core stations: Camp Century, Dye-3, GRIP, GISP2, Renland and NorthGRIP. *Journal of Quaternary Science*, **16(4)**, 299–307.

Junge, C.E. 1963. *Air Chemistry and Radioactivity.* International Geophysics Series, vol. 4. Academic Press New York and London.

Kolb, W. 1992. *Aktivitätskonzentrationen von Radionukliden in der bodennahen Luft Norddeutschlands und Nordnorwegens im Zeitraum von 1963 bis 1990.* Report PTB-Ra-29. Physikalisch Technische Bundesanstalt, Braunschweig, Germany.

Kovaltsov, G.A., & Usoskin, I.G. 2010. A new 3D numerical model of cosmogenic nuclide ^{10}Be production in the atmosphere. *Earth and Planetary Science Letters*, **291**, 182–188.

Kubik, P.W., & Christl, M. 2010. ^{10}Be and ^{26}Al measurements at the Zurich 6 MV Tandem AMS facility. *Nuclear Instruments and Methods in Physics Research B*, **268**, 880–883.

Laj, C., Kissel, C., & Beer, J. 2004. High resolution global paleointensity stack since 75 kyr (GLOPIS-75) calibrated to absolute values. *Pages 255–265 of: Timescales of the Paleomagnetic Field*. AGU Monograph.

Lazarev, V. 2003. *The cosmogenic and anthropogenic ^{36}Cl in the environment*. PhD thesis, Technical University of Munich, Munich, Germany.

Levin, I., Naegler, T., Kromer, B., Diehl, M., Francey, R.J., Gomez-Pelaez, A.J., Schäfer, A., Steele, L.P., Wagenbach, D., Weller, R., & Worthy, D.E. 2010. Observations and modelling of the global distribution and long-term trend of atmospheric $^{14}CO_2$. *Tellus*, **62B**, 26–46.

Martell, E.A. 1966. The size distribution and interaction of radioactive and natural aerosols in the stratosphere. *Tellus*, **18(2)**, 486–498.

Masarik, J. 2010. *Environmental Radionuclides: Tracers and Timers for terrestrial processes*. Elsevier. Chap. Origin and distribution of radionuclides in the continental environment.

Masarik, J., & Beer, J. 1999. Simulation of particles fluxes and cosmogenic nuclide production in the earth´s atmosphere. *Journal of Geophysical Research*, **D104**, 12,099–13,012.

Masarik, J., & Beer, J. 2009. An updated simulation of particle fluxes and cosmogenic nuclide production in the Earth´s atmosphere. *Journal of Geophysical Research*, **114**, D11103.

Muscheler, R., Beer, J., Wagner, G., Laj, C., Kissel, C., Raisbeck, G.M., Yiou, F., & Kubik, P.W. 2004. Changes in the carbon cycle during the last deglaciation as indicated by the comparison of ^{10}Be and ^{14}C records. *Earth and Planetary Science Letters*, **219**, 325–340.

Naegler, T. 2005. *Simulating bomb radiocarbon: Consequences for the global carbon cycle*. PhD thesis, University of Heidelberg, Heidelberg, Germany.

Nishiizumi, K., Imamura, M., Caffee, M.W., Southon, J.R., Findel, R.C., & J-McAninch. 2007. Absolute calibration of ^{10}Be AMS standards. *Nuclear Instruments and Methods in Physics Research B*, **258**, 403–413.

Oerter, H., Fischer, H., & Sperlich, P. 2008. Spatial variability of δ^{18}O upstream and around the EDML drilling site. *In: Quaternary Climate: from Pole to Pole, EPICA Open Science Conference, Venice, Itly, November 10-13.*

Oerter, H., Wilhelms, F., Hansson, M., Holmlund, P., Ingwander, S., Karlin, T., & Fujita, S. 2011. Stable isotope content and snow accumulation between 1964 and 2007/08 along the ice divide from Kohnen-Station towards Dome Fuji, East Antarctica. *EGU General Assembly 2011, Vienna, Austria.-8. April 2011.*

Oeschger, H., Siegenthaler, U., Gugelmann, A., & Schotterer, U. 1975. A box-diffusion model to study the carbon dioxide exchange in nature. *Tellus*, **27**, 168–192.

Papastefanou, C. 2008. *Radioactive Aerosols*. Radioactivity in the environment, vol. 12. Elsevier.

Rasmussen, S.O., Andersen, K.K., Svensson, A.M., Steffensen, J.P., Vinther, B.M., Clausen, H.B., Siggaard-Andersen, M.-L., Johnsen, S.J., Larsen, L.B., Dahl-Jensen, D., Bigler, M., Röthlisberger, R., Fischer, H., Goto-Azuma, K., Hansson, M.E., & Ruth, U. 2006. A

new Greenland ice core chronology for the last glacial termination. *Journal of Geophysical Research*, **111**, D06102.

Rasmussen, S.O., Seierstad, I.K., Andersen, K.K., Bigler, M., Dahl-Jensen, D., & Johnsen, S.J. 2008. Synchronization of the NGRIP, GRIP, and GISP2 ice cores across MIS 2 and palaeoclimatic implications. *Quaternary Science Reviews*, **27(1-2)**, 18–28.

Reimer, P.J., Baillie, M.G.L., Bard, E., Bayliss, A., Beck, J.W., Blackwell, P.G., Bronk-Ramsey, C., Buck, C.E., Burr, G.S., Edwards, R.L., Friedrich, M., Grootes, P.M., Guilderson, T.P., Hajdas, I., Heaton, T.J., Hogg, A.G., Hughen, K.A., Kromer, K.F. Kaiser B., McCormac, F.G., Manning, S.W., Reimer, R.W., Richards, D.A., Southon, J.R., Talamo, S., Turney, C.S.M., van der Plicht, J., & Weyhenmeyer, C.E. 2009. INTCAL09 and MARiNE09 radiocarbon age calibration curves, 0-50,000 years CAL BP. *Radiocarbon*, **51(4)**, 1111–1150.

Roos, P., Holm, R., Persson, R.B.R., Aarkrog, A., & Nielsen, S.P. 1994. Deposition of ^{210}Pb, ^{137}Cs, $^{239+240}$Pu, ^{238}Pu, and ^{241}Am in the Antarctic Peninsula Area. *Journal of Environmental Radioactivity*, **24**, 235–251.

Schery, S. 2001. *Understanding radioactive aerosols and their measurement.* Kluwer Academic Publishers.

Seierstad, I.K., Abbott, P., Bigler, M., Blunier, T., Bourne, A., Brook, E., Buchardt, S.L., Buizert, C., Clausen, H.B., Cook, E., Dahl-Jensen, D., Davies, S., Guillevic, M., Johnsen, S.J., Pedersen, D.S., Popp, T.J., Rasmussen, S.O., Severinghaus, J., Svensson, A., & Vinther1, B-M. 2014. Consistently dated records from the Greenland GRIP, GISP2 and NGRIP ice cores for the past 104 ka reveal regional millennial-scale isotope gradients with possible Heinrich Event imprint. *in prep. for Quaternary Science Reviews.*

Siegenthaler, U. 1983. Uptake of excess CO_2 by an outcrop-diffusion model ocean. *Journal of Geophysical Research*, **88(C6)**, 3599–3608.

Smart, D.F., & Shea, M.A. 2008. World grid of calculates cosmic ray vertical cutoff rigidities for Epoch 1995.0. *Proceedings oft he 30th International Cosmic Ray Conference Mexico City*, **1(SH)**, 733–736.

Sportisse, B. 2007. A review of parameterizations for modelling dry deposition and scavenging of radionuclides. *Atmospheric Environment*, **41**, 2683–2698.

Stanzick, A. 2001. *Raum-Zeit-Variationen von Be-10, Pb-210 und Cl-36 in der grönländischen Firndecke: Luft-Firn-Transfer und rezente Trends.* PhD thesis, Institut für Umweltphysik, University of Heidelberg.

Stohl, A. 2006. Characteristics of atmospheric transport into the Arctic troposphere. *Journal of Geophysical Research*, **111**, D11306.

Stone, J., Fifield, K., Beer, J., Vonmoos, M., Obrist, C., Grajcar, M., Kubik, P., Muscheler, R., Finkel, R., & Caffee, M. 2004. Co-precipitated silver-metal oxide aggregates for accelerator mass spectrometry of ^{10}Be and ^{26}Al. *Nuclear Instruments and Methods in Physics Research B*, **223-224**, 272–277.

Svensson, A., Andersen, K.K., Bigler, M., Clausen, H.B., Dahl-Jensen, D., Davies, S.M., Johnsen, S.J., Muscheler, R., Rasmussen, S.O., Röthlisberger, R., Seierstad, I., Steffensen, J.P., & Vinther, B.M. 2008. A 60000 year Greenland stratigraphic ice core chronology. *Climate of the Past*, **4**, 47–57.

Svensson, A., Bigler, M., Blunier, T., Clausen, H.B., Dahl-Jensen, D., Fischer, H., Fujita, S., Goto-Azuma, K., Johnsen, S.J., Kawamura, K., Kipfstuhl, S., Kohno, M., Parrenin, F., Popp, T., Rasmussen, S.O., Schwander, J., Seierstad, I., Severi, M., Steffensen, J.P., Udisti, R., Uemura, R., Vallelonga, P., Vinther, B.M., Wegner, A., Wilhelms, F., & Winstrup, W. 2013. Direct linking of Greenland and Antarctic ice cores at the Toba eruption (74 ka BP). *Climate of the Past*, **9**, 749–766.

UNSCEAR. 2000. *Sources and effects of ionizing radiation, UNSCEAR 2000 Report to the General Assembly.* Tech. rept. United Nations Scientific Committee on the Effects of Atomic Radiation, http://www.unscear.org/, Vienna, Austria, 2000.

Usoskin, I.G., & Kovaltsov, G.A. 2008. Production of cosmogenic ^{7}Be isotope in the atmosphere: Full 3-D modeling. *Journal of Geophysical Research*, **113**, D12107.

Usoskin, I.G., Galina, A., Bazilevskaya, A., & Kovaltsov, G. A. 2011. Solar modulation parameter for cosmic rays since 1936 reconstructed from ground-based neutron monitors and ionization chambers. *Journal of Geophysical Research*, **116**, A02104.

Vinther, B.M., Clausen, H.B., Johnsen, S.J., Rasmussen, S.O., Andersen, K.K., Buchardt, S.L., Dahl-Jensen, D., Seierstad, I.K., Siggaard-Andersen, M.-L., Steffensen, J.P., Svensson, A.M., Olsen, J., & Heinemeier, J. 2006. A synchronized dating of three Greenland ice cores throughout the Holocene. *Journal of Geophysical Research*, **111**, D13102.

Wagner, G. 1998. *Die kosmogenen Radionuklide ^{10}Be und ^{36}Cl im Summit-GRIP-Eisbohrkern.* PhD thesis, ETH Zurich.

Wagner, G., Beer, J., Masarik, J., Muscheler, R., Kubik, P.W., Mende, W., Laj, C., Raisbeck, G.M., & Yiou, F. 2001. Presence of the Solar de Vries Cycle (∼205 years) during the Last Ice Age. *Geophysical Research Letters*, **28(2)**, 303.

Wershofen, H., & Arnold, D. 2005. *Radionuclides in ground-level air in Braunschweig - report of the PTB Trace Survey Station from 1998 to 2003.* PTB-Ra-45. PTB Braunschweig.

Wolff, E.W., Chappellaz, J., Blunier, T., Rasmussen, S.O., & Svensson, A. 2010. Millennial-scale variability during the last glacial: The ice core record. *Quaternary Science Reviews*, **29**, 2828–2838.

Yiou, F., Raisbeck, G.M., Baumgartner, S., Beer, J., Hammer, C., Johnsen, S., Jouzel, J., Kubik, P.W., Lestringuez, J., Stievenard, M., Suter, M., & Yiou, P. 1997. Beryllium 10 in the Greenland Ice Core Project ice core at Summit, Greenland. *Journal of Geophysical Research*, **102 (C12)**, 26,783–26,794.